Submitted to PASP

Imaging With STIS: Astronomy at V = 30

Michael D. Gregg[1] & Dante Minniti[1]
Institute for Geophysics and Planetary Physics, L-413
Lawrence Livermore National Laboratory, Livermore, CA 94550
E-mail: gregg, dminniti@llnl.gov

ABSTRACT

In February, 1997, the second Space Shuttle servicing mission to the Hubble Observatory will install the Space Telescope Imaging Spectrograph (STIS). This new instrument will greatly enhance the spectroscopic capabilities of the Hubble Space Telescope by providing a longslit format and CCD detector technology. STIS can also be used as an imager, providing an alternative to the Wide Field Planetary Camera 2. The filter set of STIS is limited and does not contain standard bandpasses, but we show here that this does not preclude useful broad band photometry. In fact, the STIS photometric system may be preferable to that of WFPC2 for certain applications where a faint limiting magnitude and fine spatial resolution are overriding considerations.

The two optical wide-band choices on STIS are a clear aperture and a longpass ($\lambda > 5500$Å) filter. We define an effective shortpass filter from the difference of these, making two-color photometry possible with STIS. We present preliminary transformations between the STIS system and Cousins BVRI bandpasses, showing that these transformations are very well-behaved over almost all temperatures, luminosities, and abundances for normal stars. In an 8-orbit cycle, STIS will be able to reach signal-to-noise of $\sim 5 - 10$ at V = 30.0 in its clear and longpass imaging modes, a significant increase in the power of HST to address a number of fundamental issues out of reach of current instrumentation capabilities on the ground or in space.

Subject headings: Photometry

1. Introduction

With its combination of high angular resolution and modern CCDs, the Hubble Space Telescope has recently achieved the new world record for deep imaging in the Hubble Deep Field project (Williams et al. 1996). By integrating for $\sim 100,000$ seconds with the Wide Field Planetary Camera 2 (WFPC2), objects at 30^{th} magnitude in the F606W (roughly V) filter have been detected with S/N of 3 to 4. The second Space Shuttle servicing mission to HST is scheduled for early in 1997. One of the new instruments to be placed aboard HST is the Space Telescope Imaging Spectrograph (STIS). Although it is much anticipated as a two-dimensional spectrograph, its imaging capabilities will be extremely useful. In this paper, we explore the photometric possibilities of STIS, deriving a synthetic calibration. We argue that where a faint limiting magnitude is the overriding criterion, STIS will be superior to WFPC2. Even though STIS has a very limited filter set in the optical, we show that it can be exploited to provide useful broad band color information to unprecedented depth. Even considering the August 1996 announcement that throughput will be 30% below the original expectations, STIS is still expected to reach ~ 1.5 magnitudes fainter than WFPC2 for a given integration time. This brings the solutions to a range of heretofore unaddressable problems within reach and holds out the possibility that astronomy at V = 30 will become regular with HST.

2. Definition of the STIS Wide-Band Photometric System

The STIS CCD is a SITe 1024x1024 thinned CCD with 21μ pixels and a 16 bit analog-to-digital converter. The focal plane scale is $0\farcs05$ per pixel. The FWHM is close to 2 pixels at 5000Å, and the 90% encircled energy radius is 3 pixels. The STIS Instrument Handbook notes that the point spread function is expected to degrade by 30% at the extreme top and bottom of the field of view. Complete details of STIS as an imager can be found in the STIS Instrument Handbook (Baum et al. 1996).

The STIS imaging filter set includes a clear aperture, officially named 50CCD, with a field of view of $50''$x $50''$. Also available is a longpass ($\lambda > 5500$Å) filter, officially named F28x50LP, which has a field of view of $28''$x $50''$. We refer to these two bands simply as CL and LP, respectively. The response curve of the CL bandpass is set entirely by the telescope throughput and CCD sensitivity. The response of the LP bandpass is very similar to the CL, only slightly lower, at all wavelengths longer than 5500Å. Below this wavelength, the LP throughput is essentially zero (Figure 1; see also Figure 5.3 in the STIS Instrument Handbook).

The close match of the two bandpasses longward of 5500Å is fortuitous because it allows an effective shortpass (SP) filter and (SP-LP) color to be defined based on differencing the CL and LP bandpasses. The STIS broad band photometric system is then given by

$$\begin{aligned} CL &= -2.5log(F_{CL}) + C_{CL}, & (1)\\ LP &= -2.5log(F_{LP}) + C_{LP}, & (2)\\ SP &= -2.5log(F_{CL} - F_{LP}) + C_{SP}, \quad \text{and} & (3)\\ SP - LP &= -2.5log(\tfrac{F_{CL}-F_{LP}}{F_{LP}}) + C_{SPLP}. & (4) \end{aligned}$$

where F_{CL} and F_{LP} are the total counts for an object in each bandpass, and the C_i are zeropoint constants. This very wide-band system resembles to some extent that used successfully by the MACHO collaboration to discover and monitor microlensing events (e.g. Alcock et al. 1995). The MACHO filter system has been calibrated on to standard systems and has produced accurate photometry and color-magnitude diagrams. The slight mismatch between the CL and LP bandpasses (Figure 1) means that the SP bandpass has a small red leak, but in what follows, this does not appear to be significant except for the very reddest stars.

3. Synthetic Calibration of STIS Photometry

To investigate the utility of the STIS photometric system, we have derived transformations between the STIS magnitudes and (SP-LP) color and the Cousins wide-band system by convolving the Bruzual et al. spectrophotometric stellar library with the sensitivity curves (normalized) for the CL and LP bandpasses that are given in Chapter 14 of the STIS Instrument Handbook. We have set the zeropoint using the Kurucz (1992) model for Vega. This procedure is similar to that used by Holtzman et al. (1995) in calibrating the WFPC2 photometric system. The transformations between (SP-LP) and many of the standard broad band colors are extremely well-behaved over much of the color range, especially (B-R), (B-I) and (V-R) (Figure 2). Stars of luminosity class V are indicated by the symbols with black dots. The solid lines in Figure 2 are cubic spline fits obtained interactively using the task CURFIT in IRAF and the RMS about each fit, excluding obvious outliers, is shown in the figure. The dotted lines have a slope of unity and are drawn for reference.

The residuals from the spline fits are displayed for each color. There is a small but clear systematic separation between dwarfs and giants for spectral types later than K5 ($SP - LP > 1.5$), but it is at a level of 0.1 magnitudes or less. This behavior is seen in transformations in other photometric systems and may even be advantageous in some

circumstances. Quantifying this refinement is beyond the scope of this analysis, but if the late dwarfs and giants do separate cleanly, then there are apparently a few errors in the luminosity classifications in the Bruzual et al. stellar library.

The most natural transformation is between (SP-LP) and (B-R), which are almost perfectly matched over the interval ($0 < B - R < 2$), where the scatter is only ± 0.02 mag. The increase in scatter for $(SP - LP) \gtrsim 2$ may be a consequence of the red leak in the SP bandpass. The transformation between (SP-LP) and (B-I), while not having a slope of 1, is well-behaved over an even larger color range.

The cubic spline fits make it difficult to supply transformation equations in a concise manner. Instead, a look-up table is given in steps of 0.1 magnitudes in $(SP - LP)$ for converting to Cousins broad band colors (Table 1). An electronic version of this table, in steps of 0.01 magnitudes, is available from the authors.

In Figure 3, we plot comparisons of the difference between SP, CL, and LP magnitudes with Cousins B, V, R, and I as a function of $(SP - LP)$. The lines are cubic spline fits and, as above, the RMS is given in the figure. Again, the comparison shows that well-behaved transformations exist over almost all spectral types. For stars earlier than mid-M, the RMS scatter is only ~ 0.02 magnitudes in all bands. Here too, rather than supply a transformation equation, we simply list in Table 1 the differences between the STIS magnitudes and Cousins B, V, R, and I as given by the spline fits plotted in Figure 3.

The Bruzual et al. stellar library contains spectra of stars mainly of solar metallicity and luminosity class V and III covering all spectral types. Figures 2 and 3 demonstrate that there is a small separation by luminosity class in the STIS colors, of a few hundredths to a tenth of a magnitude, mainly for spectral types later than K5. We have also tested for possible metallicity effects using the model spectral energy distributions of Kurucz (1992). Figure 4 shows $(B - R)$ and $(SP - LP)$ for models covering the the temperature range 3500 to 50000 K at two extreme abundances, [M/H]$= -2.0$ (crosses) and $+0.5$ (triangles). There is a small difference for stars with $1 < (SP - LP) < 2$ at the level of a few hundredths of a magnitude. For the very reddest models, there is a larger difference in the transformation, but this may be a shortcoming of the models. The solid line in Figure 4 is a spline fit to the data shown in Figure 2; this fit clearly tracks the [M/H]$= -2.0$ models better than the higher metallicity ones, even though the observed stars are approximately solar abundance. The spline fit to the observed stars also differs systematically at the blue end, but here too only at the few hundredths of a magnitude level, perhaps also indicating minor difficulties with the theoretical spectral energy distributions.

These derived zeropoints and transformations do not completely substitute for an

empirical calibration of the STIS passbands on board HST when precise sensitivity functions and throughput can be determined, but they do demonstrate that STIS is useful for broad band photometry and that well-determined transformations to the standard Cousins passbands exist. Given the well-determined and calibrated transformations between the Cousins system and that of WFPC2 (Holtzman et al. 1995), there is no doubt that transformations between STIS and WFPC2 will also be equally well-behaved. This raises the possibility of using the unprecedented deep imaging capability and spatial resolution of STIS for a number of problems that cannot be addressed with current instrumentation.

One of the most important applications of broad band photometry is to construct color-magnitude diagrams for stellar systems to derive ages and abundances. The transformations derived here make it possible to place isochrones calculated in Cousins bandpasses on the STIS system, as Holtzman et al. did for the WFPC2 filters. We have mapped the New Yale Isochrones (Demarque et al. 1996) to the STIS photometric system. As examples, Figure 5 shows solar and 1/100 solar metallicity isochrones for 5, 10, and 15 Gyrs in the STIS CL vs. (SP-LP) plane. Because of the extremely well-behaved transformations, the isochrones in the STIS system are completely normal in appearance, their utility undiminished.

4. STIS Imaging Exposure Time Calculator

We have written a program to make careful estimates of the expected S/N for STIS in imaging mode. The program convolves spectrophotometry of representative stars from the Bruzual et al. library with the STIS CL and LP sensitivity functions, summing over each bandpass to obtain a count rate. Given the known instrumental characteristics of STIS, the S/N can be estimated using equations from the STIS Handbook, pp. 70-71. We have reduced the listed sensitivities by 30% as advised in the August STIS Instrument Handbook update.

Our estimates indicate that, given a low sky background and working in relatively uncrowded fields, a S/N level of 5 can be reached for a total exposure time of approximately 16000 seconds in the CL band and 21500 seconds in LP for a G5V star with V = 30.0. The S/N achieved in SP will be lower because the errors in both CL and LP contribute in quadrature. The color $(SP - LP)$ is doubly sensitive to the error in LP (Equation 4). We have taken into account that CL exposures will be limited to 900 seconds to avoid the possibility of UV damage to the CCD (STIS Instrument Handbook). The extra noise from the frequent reads has an impact on the CL S/N and has the effect of nearly equalizing the exposure times between the two bands for longer total exposures to reach a given S/N.

Although these exposure times are lengthy, they can be accommodated in two 8-orbit intervals between passages of HST through the South Atlantic Anomaly.

This faint magnitude limit reached by STIS exceeds that of WFPC2 because of several contributing factors: 1) the STIS CCD has 1.5 times the quantum efficiency of the WFPC2 CCDs, 2) the STIS CCD has lower readout noise, and 3) the STIS passbands are much broader than any of the WFPC2 filters. Compared to the imaging S/N calculation examples in the STIS Handbook, our detailed estimates are conservative by $\sim 10 - 15\%$, even after taking into account the reduction in sensitivity described in the August 1996 Update. This is likely due to adopting a more conservative point spread function for calculating the fractional energy received within the measured aperture. This may be appropriate because of the two additional sources of noise described in the August 1996 update to the STIS Instrument Handbook of fringing at $\lambda > 7000$Å, and "halos" around red objects at the 10^{-3} to 10^{-4} level. The full ramifications of these effects on S/N will not be understood until STIS is calibrated and evaluated on board HST.

We stress the need for a space-based empirical calibration of STIS photometry. Because of the unusually wide wavelength coverage of the STIS passbands and the sensitivity down to well below the atmospheric cutoff in the CL band, the STIS system will be extremely difficult to calibrate reliably from the ground. An absolute calibration of the STIS photometric system from space will be needed to take full advantage of its potential. Such calibrations can be done with a small amount of HST time and will prove useful for a wide range of projects which make use of STIS photometry. One possibility is to image a grid of fields in Galactic globular clusters which have accurate ground-based Cousins BVRI and space-based WFPC2 wide filter photometry. The clusters should span as much range in metallicity as possible to establish the exact color transforms and zeropoints. Such images would include thousands of stars each, which, combined with archival WFPC2 images, would provide all the needed zeropoint and transformation data and would even allow exploration of second order metallicity and luminosity effects.

5. Summary

The advent of STIS imaging on HST promises to open new frontiers for investigation which are beyond the reach of current instrumentation, either in space or on the ground. Although the bandpasses for optical imaging on STIS are limited, the analysis presented here demonstrates that meaningful two-color photometry is possible. The unusually wide bandpasses of STIS are in fact an advantage, allowing photometry to unprecedented depth to be brought to bear on a number of fundamental questions.

There are many areas where STIS imaging can have a significant impact. We mention a few examples, which by no means cover all the fields that could be impacted. The reader's imagination is left to consider further possibilities.

• *Main Sequence Turnoff Throughout the Local Group*

The star formation history of Local Group galaxies is varied (Hodge 1989; Da Costa 1995). With the new imaging capabilities of STIS, the main sequence turnoff's of all Local Group galaxies are now within reach, offering the possibility of directly probing the ages of objects which collapsed from primordial clouds independent from the Milky Way. The deepest photometry to date in M31 is from WFPC2 (e.g., Fusi-Pecci et al. 1996; Holland, et al. 1996) which extends 1 magnitude below the horizontal branch. The oldest main sequence turnoff of the halo of M31 (true distance modulus 24.4; Freedman & Madore 1990), for example, will be at V $\approx$ 29.0 for a $t \sim 15$ Gyr, solar abundance population (cf. Figure 5). Deep STIS exposures with the clear aperture and longpass filter will yield 6–12σ magnitudes at $V = 29$, and would allow the turnoff to be estimated to 0.1–0.2 mag with an age resolution of $\sim 2 - 3$ Gyr. Knowing the turnoff ages for many Local Group galaxies would effectively document the star formation history of a wide range of galaxy types and probe directly the formation process of the Local Group in particular and galaxies in general.

• *Cepheids in the Coma Cluster*

The debate over the Hubble constant continues to rage (Kennicutt, Freedman & Mould 1995) with recent values ranging from $56 - 58 \pm 4$ km s^{-1} Mpc^{-1} (Sandage et al. 1996) to 81 ± 6 km s^{-1} Mpc^{-1} (Tonry et al. 1996), differing at the 4σ level. With STIS, it will be possible to detect and phase Cepheids at cosmological distances where the peculiar velocities of individual galaxies and clusters are insignificant compared to the smooth Hubble flow. There is consensus in the literature on the Cepheid distance scale, so a measure of Cepheid distances to spirals in clusters out to the distance of Coma cluster would go a long way toward reducing the present uncertainty in the Hubble constant. STIS two-color photometry can be used effectively to positively identify and phase Cepheids, and to measure their reddening. If the Hubble constant is high, 70-80 km s^{-1} Mpc^{-1}, then the Coma cluster is $\sim$ 90 to 100 Mpc distant, corresponding to a distance modulus of $\sim$ 34.8 to 35. Cepheid variables with periods of 50-65 days have mean $M_V = -6$ to -6.3. For an 8 orbit integration in CL, our exposure time calculator estimates that these variables could be measured with S/N 6 to 13 at mean light. This is comparable to the S/N achieved for the shortest period (lowest luminosity) Cepheids measured in Virgo cluster spirals (Ferraresce et al. 1996). For a number of Cepheids in even a single spiral in the Coma cluster, such observations can produce a Hubble constant good to 10% or better.

• *Red Giant Branch Tip in Early Type Galaxies out to Virgo*

Stellar population studies of giant early type galaxies, ellipticals in particular, are hampered by the lack of nearby examples which can be studied star-by-star. Several analogs are often used, such as the bulges of spirals or dwarf ellipticals in the Local Group. Our understanding of the evolution of early type systems is critical for deriving q_o and, to some extent, even H_o. STIS, with the help of the Near Infrared Camera and Multi-Object Spectrograph (NICMOS, Axon et al. 1996), also scheduled to be installed in the same HST servicing mission, can make a dramatic improvement in the ability to probe directly the stellar populations in giant ellipticals. The tip of the red giant branch for old populations has $M_I \approx -4$ and $M_H \approx -7$; to measure this well, it is necessary to go at least 2 magnitudes fainter with some precision. Establishing the nature of the upper red giant branch would set limits on the metallicity and metallicity spread, the presence of intermediate age populations, and the distance to early type galaxies. With 15 orbits of integration, color-magnitude diagrams for the upper giant branch can be observed with STIS LP and NICMOS H in ellipticals out to Virgo cluster distances ($\mu \approx 31.1$), offering the chance to begin detailed investigation of the brightest stellar populations in early type galaxies.

• *Baryonic Dark Matter in Nearby Galaxies*

Velocity dispersions of nearby dwarf spheroidal galaxies are generally larger than can be accounted for with normal stellar populations, and it is believed that dwarf spheroidal galaxies contain substantial amounts of dark matter (e.g. Aaronson 1983, Mateo et al. 1991). Deep STIS imaging could probe deep enough down the main sequence (down to a few $\times 0.1$ $M_\odot$) in the nearest dwarf spheroidal galaxies such as Fornax and Ursa Minor, to test if low mass stars are the culprits. Deep luminosity functions in these systems will reveal if the mass function is skewed towards low-mass stars, contributing to our knowledge of the dark matter observed in much larger scales. Even if the mass in the lower main sequence of dwarf spheroidals is not enough to account for their unusually large velocity dispersions, establishing the mass function to such low levels has implications for both star and galaxy formation.

• *The Hubble Deep Field South*

The faint magnitude limit accessible with STIS would also allow a repeat of the Hubble Deep Field (HDF) experience (Williams et al. 1996) in a more economical manner in the Southern hemisphere. Only 16 orbits total for both CL and LP in the continuous viewing zone would be needed to achieve the same limiting magnitudes as the HDF -North-, although limited to only the two bandpasses and smaller field of view of STIS. If a total of

150 orbits were also allocated to the HDF South, then either the areal coverage could be increased over a single STIS field or the magnitude limits could be pushed even fainter than the HDF North, reaching S/N ~ 5 at V= 31.0 for a 100,000 second integration. Additional color information could be obtained with parallel NICMOS observations, perhaps of the same pieces of sky by dividing the time between two fields separated by the STIS - NICMOS focal plane distance and flipping the telescope 180° between observations.

We would like to thank our collaborators K. Cook, E. Olszewski, M. Mateo, and G. Da Costa for guidance and discussions. We are grateful to the STIS Science team headed by S. Baum and the Help Desk at STScI headed by D. Golombek for their prompt replies to our inquiries.

REFERENCES

Aaronson, M. 1983, ApJ, 266, L11

Alcock, C., et al. (The MACHO Collaboration), 1995, AJ, 59, 1653

Axon, D.J., Calzetti, D., MacKenty, J.W., Skinner, C. 1996, "NICMOS Instrument Handbook", Version 1.0 (Baltimore: STScI)

Baum, S., et al. 1996, "STIS Instrument Handbook", Version 1.0 (Baltimore: STScI)

Bruzual, Persson, Gunn, Stryker Stellar Atlas, from the STScI database

Da Costa, G. 1995, in "The Local Group", eds. Layden & Storm (Garching: ESO), p. 101

Demarque, P. 1996, private communication

Ferrarese, L., et al. 1996, ApJ, 464, 568

Freedman, W.L., & Madore, B.F. 1990, ApJ, 365, 186

Fusi-Pecci, F. et al. 1996, AJ, 112, 1461

Hodge, P. 1989, ARAA, 27, 139

Holtzman, J. A. et al. 1995, PASP, 107, 156

Kennicutt, R.C., Freedman, W.L., & Mould, J.R. 1995 AJ, 110, 1476

Kurucz, R.L. 1992, private communication

Holland, S., Fahlman, G., & Richer, H. 1996, AJ, in press (astro-ph/960678)

Mateo, M., Olszewski, E. W., Welch, D. L., Fischer, P., & Kunkel, W. 1991, AJ, 102, 914

Sandage, A., Saha, A., Tammann, G.A., Labhardt, L., Panagia, N., & Macchetto, F.D. 1996, ApJL, 460, L15

Tonry, J.L., Blakeslee, J.P., Ajhar, E.A., & Dressler, A. 1996, in press, astro-ph/9609113

Williams, R.E., et al. 1996, AJ, 112, 1335

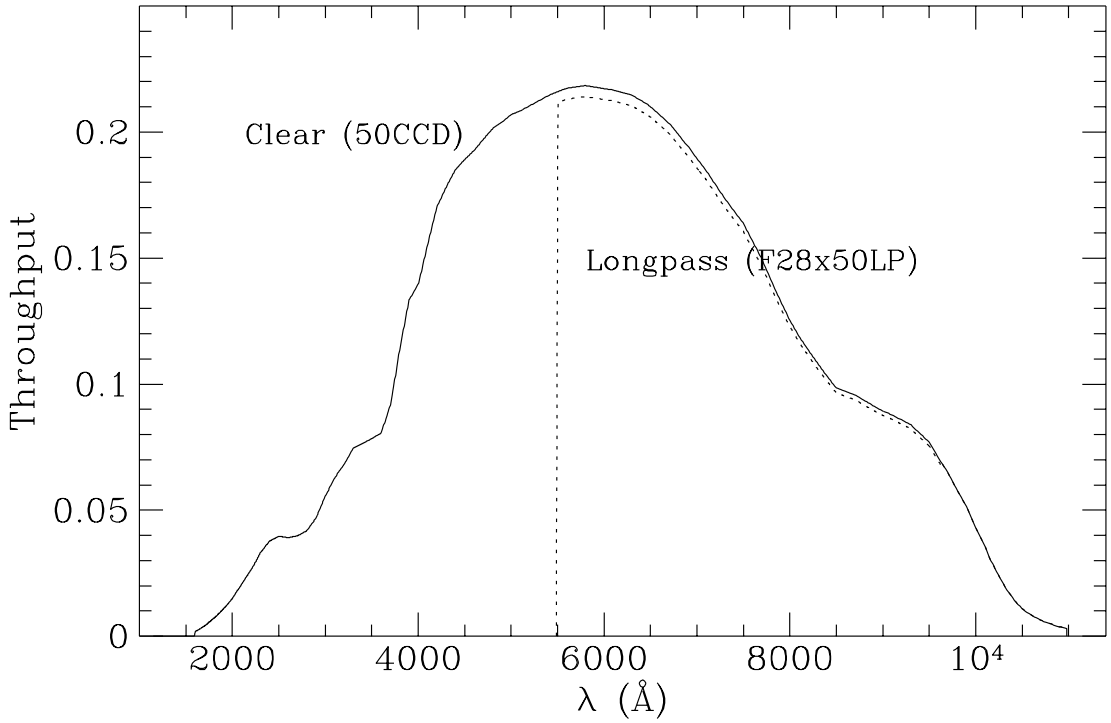

Fig. 1.— Throughput of the STIS wide bandpasses as given in the STIS Instrument Handbook. The Clear 50CCD (CL) curve is shown by the solid line and the Long Pass F28x50CCD (LP) is the dotted line. Note the close similarity of the two everywhere the LP transmits.

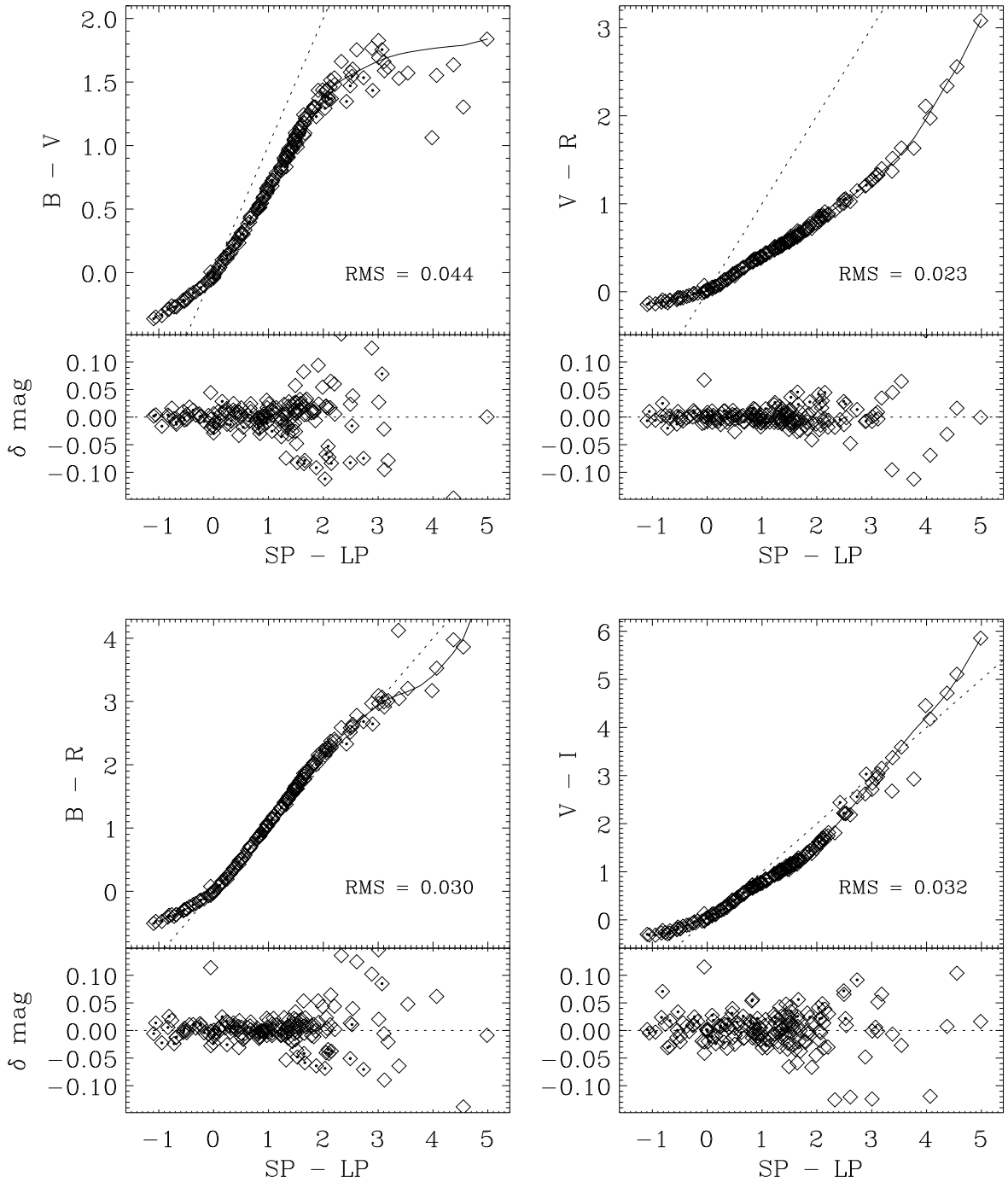

Fig. 2.— Transformations of the STIS broad band color, $SP - LP$, to standard Cousins filters, determined by convolving the STIS sensitivity functions with the spectral energy distributions of 175 stars from the spectrophotometric library of Bruzual et al. Dwarfs are indicated by the symbols containing black dots. The dashed lines have a slope of unity. The best transformations are between $SP - LP$ and $B - R$ or $B - I$. There is a small systematic difference in the transformations for stars later than spectral type K5 ($SP - LP > 1.5$), but it is at the few hundredths of a magnitude level.

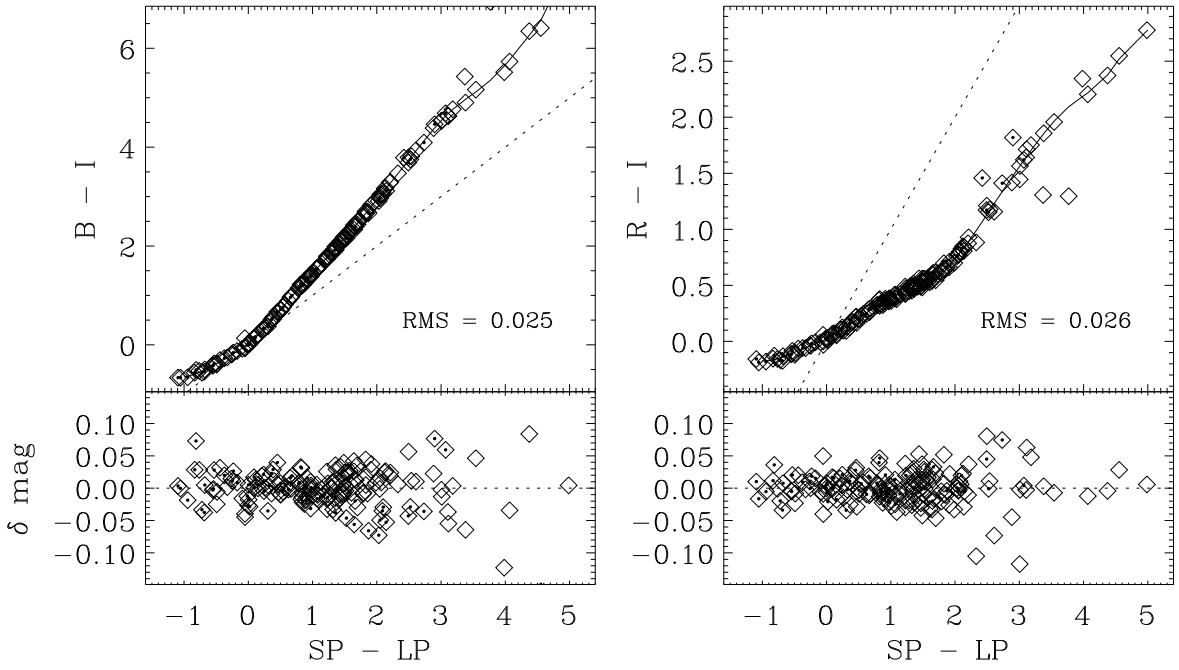

Fig. 2.— Figure 2 cont'd

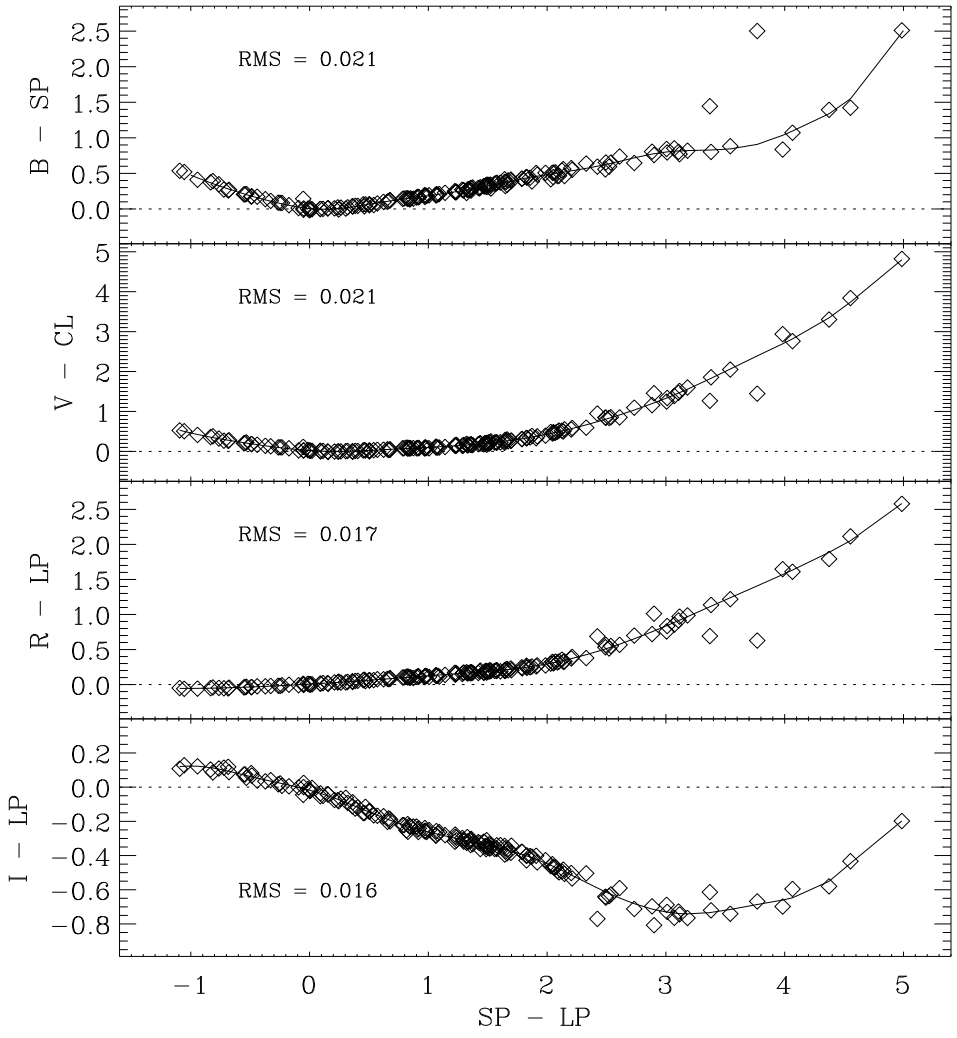

Fig. 3.— Transformation of the STIS band passes SP, CL, and LP to standard Cousins B, V, R, and I, as a function of (SP–LP) determined from the spectral energy distributions of 175 stars from the spectrophotometric library of Bruzual et al. The Kurucz (1992) model of Vega is used to set the zeropoint

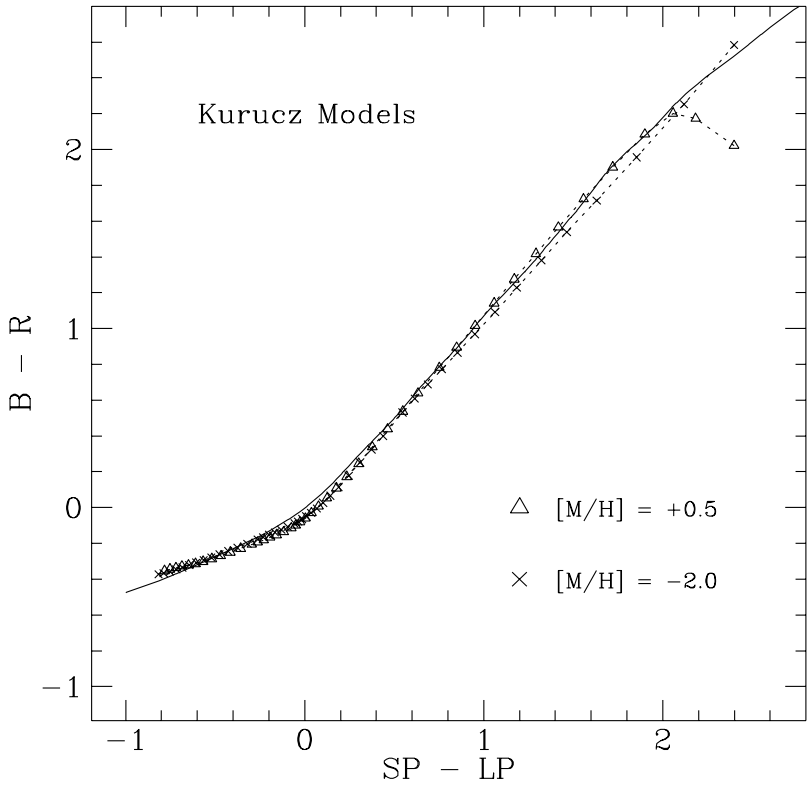

Fig. 4.— Transformations of the STIS broad band color, $SP - LP$, to standard Cousins filters, for Kurucz model atmospheres for two abundances, [M/H]= −2.0 and +0.5. Any metallicity affects in the transformation are very small, at the level of a few hundredths of a magnitude. The solid line is the same spline transformation plotted in Figure 2 for stars in the Bruzual et al. spectrophotometric library between $SP - LP$ and $B - R$.

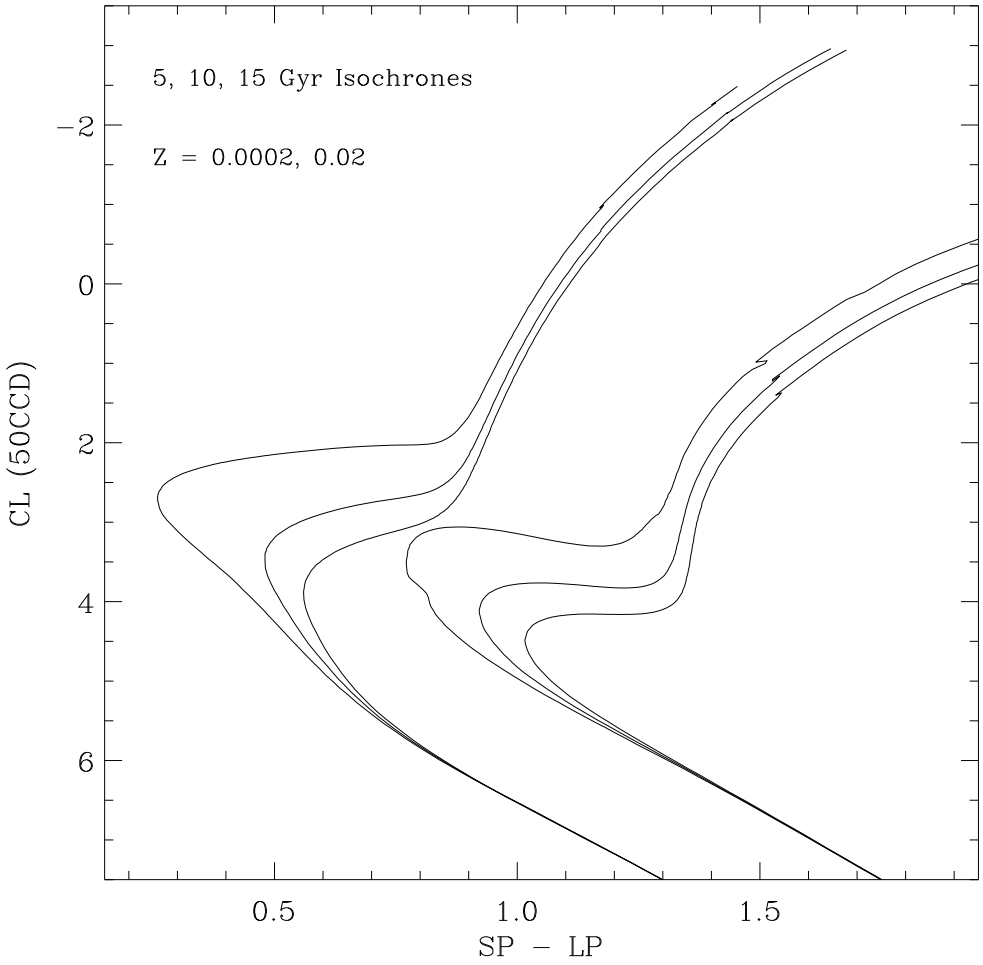

Fig. 5.— Example New Yale Isochrones (Demarque et al. 1996) transformed to the STIS photometric system. Two limiting cases are shown, metal-poor and metal-rich, for three different ages. The metal-poor turnoffs are bluer and brighter than the metal-rich turnoffs of the same age. Although the isochrones shown are unreddened, a reddening of $E_{B-V} = 0.2$ has been assumed to compute the S/N = 5 line drawn. We have also computed the dependence of S/N with color, and it is nearly flat as indicated.

Table 1. STIS to Cousins Interpolation Table

SP–LP	B–V	V–R	B–R	V–I	B–I	R–I	B–SP	V–CL	R–LP	I–LP
-1.000	-0.338	-0.134	-0.471	-0.312	-0.650	-0.173	0.475	0.463	-0.054	0.123
-0.900	-0.311	-0.127	-0.437	-0.307	-0.618	-0.171	0.410	0.397	-0.053	0.119
-0.800	-0.286	-0.116	-0.401	-0.287	-0.573	-0.161	0.348	0.339	-0.050	0.110
-0.700	-0.262	-0.102	-0.363	-0.253	-0.516	-0.143	0.290	0.286	-0.046	0.096
-0.600	-0.237	-0.086	-0.322	-0.212	-0.449	-0.121	0.237	0.240	-0.041	0.080
-0.500	-0.211	-0.070	-0.280	-0.170	-0.380	-0.098	0.186	0.195	-0.035	0.063
-0.400	-0.180	-0.055	-0.234	-0.130	-0.309	-0.075	0.140	0.152	-0.027	0.047
-0.300	-0.145	-0.040	-0.184	-0.091	-0.235	-0.052	0.098	0.113	-0.020	0.031
-0.200	-0.105	-0.024	-0.129	-0.051	-0.156	-0.029	0.060	0.077	-0.011	0.016
-0.100	-0.062	-0.005	-0.068	-0.007	-0.069	-0.004	0.029	0.046	-0.003	-0.000
0.000	-0.013	0.017	0.001	0.042	0.028	0.023	0.006	0.022	0.007	-0.018
0.100	0.040	0.045	0.082	0.099	0.138	0.053	-0.004	0.007	0.017	-0.038
0.200	0.098	0.079	0.175	0.166	0.263	0.088	-0.000	0.000	0.027	-0.062
0.300	0.160	0.118	0.278	0.241	0.401	0.125	0.015	0.002	0.038	-0.088
0.400	0.225	0.161	0.388	0.323	0.549	0.165	0.039	0.010	0.050	-0.116
0.500	0.293	0.205	0.501	0.408	0.703	0.206	0.066	0.023	0.062	-0.145
0.600	0.364	0.250	0.616	0.492	0.859	0.246	0.093	0.038	0.074	-0.173
0.700	0.436	0.294	0.729	0.574	1.014	0.285	0.117	0.055	0.087	-0.199
0.800	0.510	0.334	0.842	0.652	1.165	0.322	0.141	0.070	0.099	-0.222
0.900	0.584	0.372	0.954	0.723	1.310	0.355	0.164	0.085	0.112	-0.243
1.000	0.658	0.407	1.064	0.791	1.452	0.387	0.186	0.100	0.125	-0.262
1.100	0.734	0.441	1.174	0.855	1.593	0.416	0.209	0.116	0.137	-0.279
1.200	0.812	0.475	1.285	0.919	1.733	0.444	0.234	0.134	0.149	-0.294
1.300	0.890	0.510	1.399	0.982	1.874	0.472	0.261	0.154	0.161	-0.309
1.400	0.970	0.548	1.517	1.047	2.017	0.499	0.292	0.179	0.174	-0.324
1.500	1.050	0.587	1.638	1.114	2.163	0.527	0.327	0.207	0.187	-0.340
1.600	1.128	0.628	1.759	1.186	2.312	0.558	0.362	0.240	0.202	-0.356
1.700	1.204	0.671	1.877	1.263	2.464	0.593	0.396	0.278	0.220	-0.375
1.800	1.274	0.714	1.989	1.347	2.619	0.634	0.427	0.323	0.241	-0.396
1.900	1.336	0.758	2.093	1.440	2.775	0.683	0.455	0.373	0.265	-0.420
2.000	1.390	0.801	2.189	1.542	2.933	0.741	0.482	0.431	0.295	-0.448
2.100	1.435	0.844	2.278	1.653	3.093	0.808	0.507	0.495	0.329	-0.479
2.200	1.472	0.888	2.358	1.773	3.255	0.883	0.534	0.565	0.369	-0.512
2.300	1.503	0.932	2.431	1.898	3.418	0.964	0.563	0.642	0.413	-0.547
2.400	1.530	0.976	2.502	2.027	3.581	1.049	0.594	0.725	0.461	-0.581
2.500	1.555	1.022	2.573	2.158	3.746	1.135	0.627	0.812	0.514	-0.615
2.600	1.578	1.069	2.648	2.290	3.910	1.222	0.665	0.905	0.571	-0.645
2.700	1.601	1.118	2.726	2.422	4.073	1.307	0.705	1.003	0.632	-0.672
2.800	1.623	1.168	2.802	2.556	4.232	1.392	0.742	1.107	0.697	-0.695
2.900	1.644	1.218	2.877	2.690	4.387	1.476	0.776	1.214	0.765	-0.716
3.000	1.664	1.270	2.942	2.827	4.532	1.558	0.800	1.330	0.835	-0.730

Table 1—Continued

SP–LP	B–V	V–R	B–R	V–I	B–I	R–I	B–SP	V–CL	R–LP	I–LP
3.100	1.682	1.322	2.997	2.967	4.665	1.639	0.814	1.452	0.908	-0.738
3.200	1.697	1.374	3.042	3.112	4.782	1.718	0.821	1.582	0.983	-0.740
3.300	1.709	1.428	3.080	3.261	4.885	1.794	0.825	1.719	1.058	-0.736
3.400	1.721	1.483	3.115	3.409	4.985	1.868	0.831	1.859	1.133	-0.730
3.500	1.730	1.545	3.145	3.558	5.078	1.936	0.840	2.003	1.208	-0.720
3.600	1.738	1.614	3.181	3.701	5.178	1.998	0.860	2.148	1.283	-0.708
3.700	1.745	1.691	3.221	3.839	5.282	2.055	0.889	2.292	1.357	-0.695
3.800	1.752	1.774	3.270	3.973	5.395	2.107	0.926	2.436	1.432	-0.682
3.900	1.758	1.872	3.338	4.096	5.529	2.149	0.986	2.578	1.507	-0.670
4.000	1.765	1.971	3.408	4.218	5.666	2.191	1.047	2.720	1.583	-0.658
4.100	1.770	2.078	3.498	4.342	5.820	2.235	1.122	2.876	1.662	-0.636
4.200	1.774	2.185	3.598	4.474	5.982	2.287	1.201	3.047	1.744	-0.605
4.300	1.779	2.291	3.698	4.607	6.144	2.339	1.280	3.219	1.826	-0.574
4.400	1.783	2.395	3.805	4.748	6.308	2.398	1.369	3.402	1.910	-0.535
4.500	1.787	2.490	3.932	4.913	6.478	2.477	1.485	3.620	2.003	-0.477
4.600	1.794	2.599	4.099	5.091	6.689	2.546	1.647	3.850	2.110	-0.419
4.700	1.805	2.724	4.313	5.285	6.948	2.604	1.862	4.096	2.232	-0.362
4.800	1.816	2.848	4.527	5.479	7.207	2.663	2.077	4.342	2.354	-0.305
4.900	1.828	2.973	4.741	5.673	7.466	2.721	2.292	4.587	2.477	-0.247
5.000	1.839	3.098	4.956	5.867	7.725	2.779	2.507	4.833	2.599	-0.190